

METHODOLOGICAL NOTES PACS numbers: 01.50.Pa, **52.35.–g**, **94.20.–y**

Demonstration of nonlinear wave phenomena in the plasma of a laboratory model of an ionospheric-magnetospheric density duct

G A Markov, A S Belov

DOI: 10.3367/UFNe.0180.201007d.0735

Contents

Abstract. **A plasma-wave discharge in a linear magnetic mirror configuration is proposed for laboratory modeling and studying of nonequilibrium magnetospheric processes producing electromagnetic radiation in a geomagnetic-field tube with an enhanced-density duct in the magnetosphere, as well as for demonstrating the ionization self-focusing and channeling of wave fields in the whistler frequency range. Nine demonstrations of nonlinear wave phenomena in the plasma of a laboratory model of an ionospheric–magnetospheric resonator with a density duct are discussed. A laboratory device is described that allows reproducing each of these demonstrations by setting appropriate experimental conditions.**

1. Introduction

Exploring electromagnetic and plasma-wave phenomena in the Earth's ionospheric–magnetospheric system is an important problem of modern physics. Interest in it is now growing, owing to an abrupt and very substantial increase in the anthropogenic electromagnetic load on the ionosphere. Determining and studying the potential of controlled influence on these phenomena is especially challenging. The feasibility of controlled influence lies in the formation of artificial waveguide channels (ducts of plasma density) in the outer ionosphere or modification of natural channels by powerful radio emission either from the Earth [1–4] or spacecraft [5, 6]. The waveguide channels contribute noticeably to local ionospheric–magnetospheric connections, modify the conditions governing the excitation and propagation of wave processes, and also favor the formation of global resonance systems.

G A Markov, A S Belov N I Lobachevsky State University of Nizhny Novgorod,
prosp. Gagarina 23, 603950 Nizhny Novgorod, Russian Federation
Tel. (7-831) 465 60 35. Fax (7-831) 465 85 92
E-mail: markov@rf.unn.ru

Received 1 December 2009, revised 30 March 2010
Uspekhi Fizicheskikh Nauk **180** (7) 735 – 744 (2010)
DOI: 10.3367/UFNr.0180.201007d.0735
Translated by S D Danilov; edited by A Radzig

The cumbersome character and high cost of space experiments aimed at exploring such phenomena in the terrestrial space explain the necessity of developing model research carried out under laboratory conditions. Since all existing similarity criteria cannot be satisfied in the laboratory [7, 8], one should, as a rule, perform qualitative modeling and focus on the two or three most essential similarity parameters that reflect the nature of the phenomenon. However, the main difficulty in laboratory modeling of such phenomena comes from the effect of the walls of a plasma chamber and the need to eliminate their impact on the phenomena to be studied. Making use of density ducts for localizing these phenomena in waveguide channels allows the influence of side walls of the discharge chamber to be reduced and modeling to be carried out with rather compact laboratory devices. In order to model effects caused by thermal and ponderomotive nonlinearity it is convenient to use a cold decaying plasma of pulse discharges. Such a plasma allows one to create artificial waveguide channels (ducts) with reduced density [9, 10], but then the sources of high-velocity particle beams are necessary to excite electromagnetic instabilities. Moreover, because of its short lifetime, such a plasma cannot be used for demonstration purposes.

This paper presents a description of a laboratory setup designed to demonstrate nonlinear wave phenomena in the plasma of a laboratory model of an ionospheric–magnetospheric density duct, produced through ionization self-channeling of plasma waves in a magnetic mirror trap. The stationary structure of high-frequency (HF) discharge, the availability of hot electrons confined in the trap, and the absence of limitations on the observation time enable one to explicitly demonstrate a set of nonlinear phenomena occurring in the plasma of an ionospheric-magnetospheric resonator with a density duct. This setup is operated at the N I Lobachevsky State University of Nizhny Novgorod for teaching and research.

It should be noted that nonlinear wave processes stimulated by the radio radiation of ground-based high-frequency (HF) heating facilities in the middle ionosphere near the reflection region of pump wave are quite thoroughly studied and described in reviews [11, 12].

A pump wave field can be used to create a lattice of plasma irregularities in the lower ionosphere; the reflection from them then serves for diagnostic purposes [13].

A substantial interest is also aroused by phenomena in the outer ionosphere, which are related to the formation of artificial waveguide channels by powerful radio emission from the Earth, and have a pronounced impact on local ionospheric–magnetospheric connections [3, 14].

Thus, there exists a fairly broad class of nonlinear phenomena which are observed in the terrestrial space if a weakly ionized plasma of the Earth's ionosphere is modified by powerful radio radiation from ground-based sources. This article deals with the feasibility of modeling and demonstrating some of them under laboratory conditions.

2. Laboratory setup for demonstrations

To demonstrate and model nonlinear wave phenomena in the plasma of a wave channel, the laboratory setup which is sketched in Fig. 1 was proposed.

The setup comprises a discharge chamber in a magnetic mirror trap. The magnetic field in the trap was generated by two solenoids (coils *1* and *2*) with separate power supplies, which enabled the longitudinal distribution $B_z(z)$ of the magnetic field induction to be varied from a quasiuniform to an essentially nonuniform distribution of mirror configuration. The distance between the mirror centers measured 120 cm. The discharge was formed in a glass tube 150 cm in length and $2a = 6$ cm in diameter as a result of ionization self-channeling [15] of wave fields in the whistler frequency range. They were generated by a quadrupole antenna made of three copper rings embracing the tube in its central part. The HF voltage ($f = 200$ MHz, $V_0 = 50$ V) was fed to the antenna excitation rings from a GST-2 oscillator via a coaxial cable. Its central core was connected to the central ring, and its metallic shield, to the side rings.

Air served as a working gas, and its pressure was adjustable at any level in the range $p \sim 10^{-1} - 10^{-5}$ Torr. The HF power injected into the discharge was about 10 W. The plasma density $\bar{N}(z)$ averaged over the cross section of the discharge column was determined with the help of a microwave (MW) interferometer at a frequency of 9.5 GHz and by the dispersion characteristics of surface waves guided by the plasma column [16]. To detect electromagnetic radiation in the plasma, an SK4-Belan spectrum analyzer was used together with a DSO Classic-6000 digital storage oscilloscope. Signals from a rod or symmetric dipole antenna were analyzed. It was located at the surface of a discharge tube along its axis and could move in the region between the coils of the magnetic mirrors.

The quadrupole HF source was specially chosen to minimize radiation emitted to the outer space. It turned out that coils of solenoids represent a slow-wave system with characteristic longitudinal scales $l_1 \approx 10 - 12$ cm and $l_2 \approx 24$ cm. The length l_a of the antenna, therefore, was chosen from the condition of a 'resonant' wave excitation: $l_{a1} \sim \lambda_1 \sim l_1$ or $l_{a2} \sim \lambda_2 \sim l_2$. It is noteworthy that the structure of the source field essentially changed as the discharge was forming. The discharge initiation is governed by the source near field, but when the plasma density in the discharge exceeds the critical one ($\omega_{pe} > \omega$), the structure of both near and far fields of the antenna in the whistler frequency range undergoes drastic modification. Resonance conical surfaces then stretch out from the antenna rings [15, 17]. The resonance growth of the HF field on these surfaces stems from the excitation of plasma (quasilongitudinal) waves with various scales (from the ring wire diameter to the scale exceeding the source size). If the electron mean free path is small ($l_e \leqslant 1$ cm), the resonance cone is well discernible with the naked eye. This implies that major HF heating of electrons and gas ionization happen near the resonance surface, i.e., the dominant share of energy supplied by the HF source is spent to excite plasma waves. A plasma column (waveguide) is formed at the focus of the resonance cone, which confines the radiation from the source along the external magnetic field direction [18, 19]. The column is detached from the walls of the discharge tube and self-localized on the source axis. Figure 2 shows the structure of the HF discharge at a relatively high air pressure in the chamber ($p \geqslant 10^{-2}$ Torr, $l_e \leqslant 3$ cm). It illustrates the focusing and self-channeling of the wave fields in the whistler frequency range.

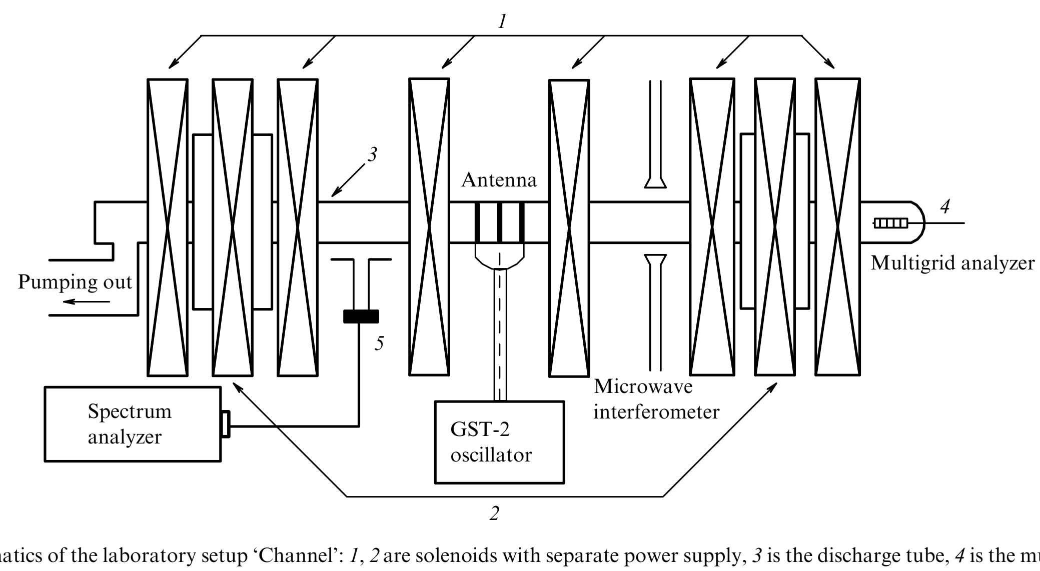

Figure 1. Schematics of the laboratory setup 'Channel': *1*, *2* are solenoids with separate power supply, *3* is the discharge tube, *4* is the multigrid analyzer, and *5* is the receiving antenna.

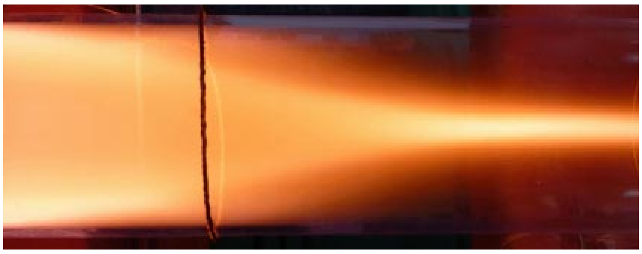

Figure 2. The structure of high-frequency discharge in a magnetoplasma ($p = 10^{-2}$ Torr): the focal region of the resonance surface of the HF source fields extending in a plasma-waveguide channel. The central excitation ring is to the left; the right grounded ring is seen in the picture.

At low pressures and large electron mean free paths ($l_e > 5$ cm), sharp plasma irregularities are smeared out along the direction of an external magnetic field and, consequently, the plasma column becomes less sharp, too. The structure of fields of the resonance cone is, however, preserved. The near (quasistatic) field of the quadrupole source decays strongly with distance from the excitation rings, so that the wave fields turn out to be much stronger than the near fields behind the focus of the resonance cone. This is proved by a narrow plasma column protruding out of the focus — the waveguide channel along which the HF energy needed to form and sustain this duct is transmitted. Small-scale plasma waves decay near the resonance surface, and the wave duct is formed and maintained by the field of waves satisfying respective dispersion relations and complying with the structure of the source field.

The peculiar features of ionization self-channeling pertaining to wave fields in the whistler frequency range in a nonuniform magnetic field of a magnetic mirror include the narrowing of the discharge plasma column in the region of strong field B_z, an increase in plasma density there, and the presence of the standing wave structure in the radiation forming the discharge channel [20]. Figure 3 depicts the axial distributions of channel radius $R_\perp(z)$ and plasma density $\bar{N}(z)$ in the trap, averaged over the channel cross section for a given distribution of the longitudinal component B_z of a magnetic field at $p = 8 \times 10^{-3}$ Torr.

An HF discharge localized on the axis of the mirror magnetic trap chamber can be conveniently used for laboratory modeling of wave and resonance processes in a magnetospheric resonator with a waveguide channel (duct) of increased plasma density. It turned out that the distribution along the trap axis of such parameters as the plasma density in the discharge channel, channel width, and the magnitude of the magnetic field is similar to that in the natural magnetospheric duct. The main drawback of the laboratory implementation of the magnetospheric resonator considered here is its linear geometry. As a result, specific features manifested by transverse diffusion of charged particles and peculiarities of electromagnetic radiation propagation in a curvilinear magnetic field, characteristic of a magnetospheric resonator, turned out to be lost.

Figure 4 shows how the amplitude squared of the longitudinal component of the electric component of the HF field forming the discharge channel varies along the outer wall of the discharge tube at a frequency of 200 MHz. The stars mark the positions of HF-antenna excitation rings. The complex structure of $|E_z(z)|^2$ is explained by the interference of the eigen wave field of the inhomogeneous plasma duct with the near field of the HF source and the waves reflected from magnetic coils with reduced inner diameter, located in the region of the mirrors, as well as from a sharp jump in plasma density near the end surface of the multigrid analyzer. An important feature in the distribution of $|E_z(z)|^2$ reproduced here is the presence of a standing structure in the wave field with typical longitudinal scales of about 10–12 cm.

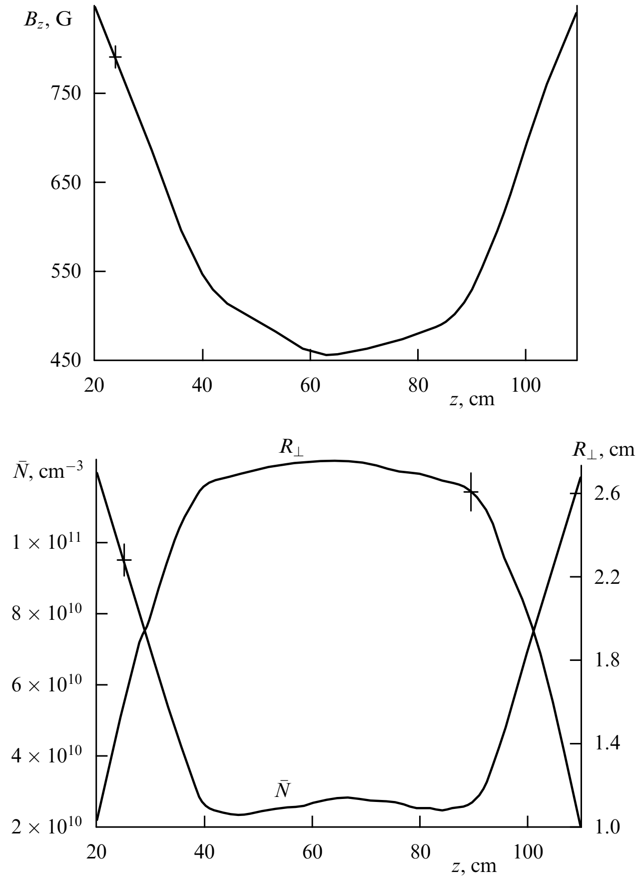

Figure 3. Distribution of the parameters $B_z(z)$, $\bar{N}(z)$, and $R_\perp(z)$ along the longitudinal axis of the setup at $p = 8 \times 10^{-3}$ Torr.

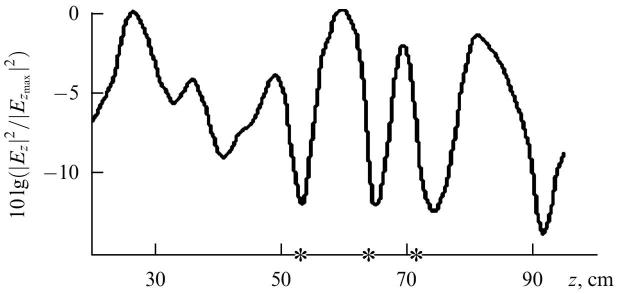

Figure 4. Square of the amplitude of the longitudinal component of the electric component of the HF field forming the discharge channel vs. the distance along the discharge tube.

3. Stimulated scattering of a wave beam forming the discharge channel in a mirror magnetic trap

Studies of electromagnetic perturbations generated in a nonequilibrium plasma of HF discharge in a mirror magnetic trap have revealed a strong sensitivity of both the spectra and

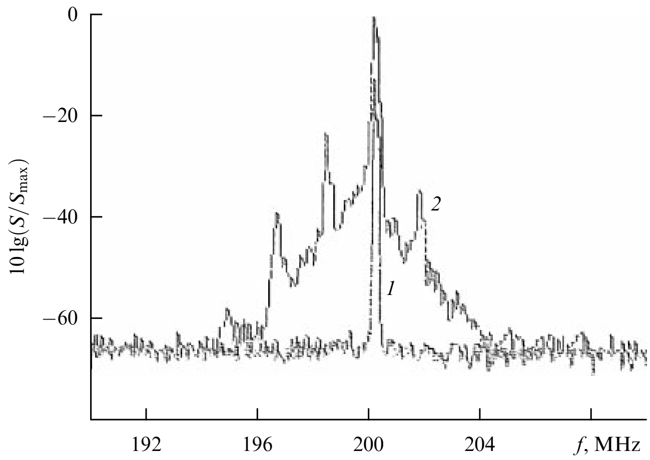

Figure 5. The spectral composition of radiation forming the discharge channel. Curve *1* corresponds to the case with no plasma load, and curve *2*, to the case when the pump field is present in the HF discharge plasma.

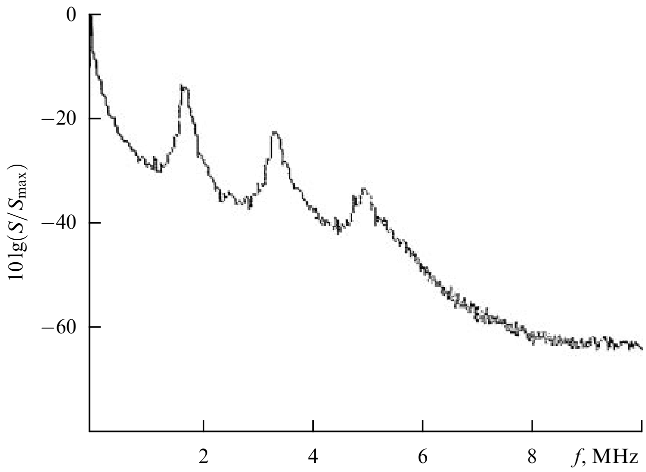

Figure 6. The dependence of the spectral power density of electric oscillations in a plasma on frequency at $p = 8 \times 10^{-3}$ Torr.

nature of occurring oscillations to the relationship between the electron mean free path l_e, trap length L, and wavelengths λ of the beam forming the discharge channel. For instance, if the pressure is sufficiently high, so that the electron mean free path becomes shorter than the wavelength of the standing wave of radiation forming the discharge channel ($l_e \leqslant \lambda/2$), the generation of ionization waves proved to be possible. They form a lattice of plasma irregularities at the antinodes of the pump standing-wave field.

The spectral composition of radiation forming the discharge channel is illustrated for this case (l_{a2}) in Fig. 5, where curve *1* corresponds to the case with the plasma load absent.

In a plasma of HF discharge, the spectral composition of the pump field (curve *2*) becomes essentially broader (especially on its 'red' side), exhibiting isolated modulation peaks. Monotonic spectral broadening stems from pump wave scattering from ion-acoustic plasma oscillations [21, 22]. The peaks are observed in a rather narrow interval of pressure, $p \approx 3 \times 10^{-2} - 5 \times 10^{-3}$ Torr, and for the magnetic field induction $B_{z0} \approx 300 - 600$ G in the central trap part. The frequency shift between the peaks, which depends on discharge conditions, varies from 1.4 MHz ($p \geqslant 10^{-2}$ Torr, $B_{z0} \approx 350$ G) to 1.8 MHz ($p < 10^{-2}$ Torr, $B_{z0} \approx 550$ G).

When exploring the low-frequency noise radiation occurring in the discharge plasma in the parameter range mentioned above, a considerable increase in noise was discovered in the frequency range up to 4 MHz, together with the appearance of well-pronounced maxima at harmonics of the lowest frequency f_0 of the fundamental mode ($f_0 \approx 1.7$ MHz at $p \approx 8 \times 10^{-3}$ Torr and $B_{z0} \approx 450$ G). Figure 6 displays the dependence of spectral power density on frequency as obtained in experiments under conditions stated above with the help of the SK4-Belan analyzer and a rod antenna located in the vicinity of the magnetic mirror ($z \approx 95$ cm). It should be noted that the amplitude of emerging peaks reaches a maximum in the vicinity of the mirrors.

A physical model corresponding to the modulation phenomena observed here is as follows. An enhanced gas ionization at the antinodes of a pump standing-wave electric field (the ionization frequency $\nu_i \sim E^{2\beta}$, where β is a quantity of order one or higher [23]) may favor the buildup of a lattice of plasma irregularities [24] with a typical spatial scale $\Lambda \approx 12$ cm. Because the lattice period is close to half the wavelength of the pump wave, the lattice buildup triggers a strong Bragg reflection. As a result, the amplitude of the wave forming the discharge reduces, the plasma irregularities smear out, reflection decreases, and the standing structure of the pump wave develops once again, bringing about plasma irregularities. This oscillatory process continues further in the same way. The time needed for inhomogeneities to form, $\tau \sim 1/\nu_i$, is around or less than that of their smearing out because of ambipolar diffusion along the magnetic field. Since diffusion toward side walls is impeded by electron magnetization, the frequency of occurring relaxation oscillations of the ionization–diffusion type is determined by the time needed for diffusive smearing out of plasma irregularities along B_z:

$$\omega_0 = 2\pi f_0 \approx D_{\mathrm{amb}} k_0^2 \approx D_{\mathrm{amb}} \left(\frac{2\pi}{\Lambda}\right)^2 . \tag{1}$$

Here, $D_{\mathrm{amb}} = k_B T_e/(m\nu_{en} + M\nu_{in})$ is the coefficient of ambipolar diffusion, T_e is the electron temperature, ν_{in} and ν_{en} are the collision frequencies of, respectively, ions and electrons with neutral molecules, and M and m are the respective masses of the ion and electron.

Choosing parameter values which correspond to the experimental conditions, viz. $T_e \approx 10$ eV, $\nu_{en} = 1.4 \times 10^8$ s^{-1}, and $\nu_{in} = 10^4$ s^{-1}, one obtains $f_0 \approx 1.7$ MHz.

When the gas pressure is reduced, the electron mean free path increases and f_0 grows to some extent; however, for $l_e > \lambda/2$ ($p < 4 \times 10^{-3}$ Torr), plasma irregularities smear out along the z-axis over distances exceeding those between the sources of enhanced ionization. As a result, the lattice of plasma irregularities disappears and, as a consequence, the maxima in the spectral characteristics of the scattered HF signal and noisy plasma low-frequency (LF) oscillations disappear, too. As the pressure is increased, the waves forming the discharge exhibit more damping, the amplitude of reflected waves reduces, and for $p > 3 \times 10^{-2}$ Torr the periodic irregularity in the distribution of $E_z(z)$ becomes insufficient for the formation of a plasma irregularity lattice.

If the amplitude of ionization–relaxation oscillations exceeds the noise level by 5 dB, the generation of harmonics

nf_0 ($n = 1, 2, 3, \ldots$) of the fundamental frequency is observed. The number of harmonics increases together with the amplitude of the fundamental harmonic ($n = 1$). Apparently, as the amplitude of the standing wave field raises, additional scales (Δl) evolve in the lattice of plasma irregularities, together with the main scale $\Lambda \approx \lambda/2$. They are caused by sharpening the plasma irregularity tips because of the nonlinear dependence of the ionization frequency on the HF field. The decay time for such 'sharp' features is smaller than $1/f_0$ by a factor of $(\Delta l/\lambda)^2$, but their occurrence frequency should be a multiple of f_0.

Relationship (1) proves to be rather helpful for diagnostic purposes. Under laboratory conditions, determining Λ, l_e, and the electron temperature is fairly easy, and Eqn (1) can be exploited to determine the ion temperature, which is routinely estimated in a very rough manner by the temperature of the walls of the discharge chamber.

When exploring the ionosphere with the help of radiation from heating facilities [13, 25], the diagnostics of plasma parameters in the ionospheric region between the E and F layers by the spectrum of the scattered signal become possible, which is difficult to achieve with other radiophysical means. It should be noted that the lattice of irregularities in an equilibrium cold plasma of the lower ionosphere is also formed when $l_e \leqslant \lambda/2$ through nonuniform heating of electrons in the field of a pump standing wave.

4. Generation of electromagnetic oscillations at frequencies of lower hybrid and bounce resonances

The generation of extremely low-frequency (ELF) radiation in the Earth's magnetosphere is commonly attributed to the resonant interaction of Alfvén and whistler waves with charged particles of radiation belts, drifting in the inhomogeneous magnetic field [26]. Ducts of plasma density localize the excitable electromagnetic fields in a narrow geomagnetic tube. Provided that the duct length is long enough, the requirements for the intensity of fast particle beams needed to excite the magnetospheric resonator can become essentially less limiting.

In this section we present the results of laboratory modeling pertaining to the effects from the excitation of instabilities in the Earth's magnetosphere at frequencies of bounce-oscillations of fast electron beams between magnetic mirrors, and in the vicinity of lower hybrid resonance. Because of the thermal spread in electron velocities, these oscillations have a noisy character. However, in a low-pressure discharge (the electron mean free path exceeds the length of the resonator), the presence of electron beams with sufficiently high intensity manifested itself in noisy emissions in the form of intensity maxima at bounce frequencies which correspond to a characteristic energy of electrons in the discharge. A noticeable increase in intensity of these oscillations was recorded at eigenfrequencies of electromagnetic oscillations in the inhomogeneous plasma column. For example, an increased level of noise emission was observed at frequencies lying in the lower hybrid resonance band [27].

Detection of electromagnetic oscillations in the plasma column is possible with the help of a dipole antenna attached to the surface of discharge tube *5* (see Fig. 1), and multigrid analyzer *4* at the end of the tube. Signals from the antenna and analyzer pass to an SK4-Belan spectrum analyzer, and the effects under study are demonstrated on its screen.

A characteristic shape of the noise radiation spectrum is a broadband line, the intensity of which decreases monotonically with increasing frequency. Understandably enough, in the general case one deals with nonequilibrium (quasiequilibrium) noise — the particle distribution function in a discharge plasma is not an equilibrium one, as evidenced by electron spectra measured with the multigrid analyzer. Measurements have indicated that the electron distribution function in the discharge plasma strongly deviates from the Maxwellian one in the energy range above 10 eV. The nonequilibrium character of plasma was sustained by a fraction of hot discharge electrons which were confined in the trap because of a large transverse velocity component.

Figure 7 presents the retardation curve $I_e(V)$ for discharge electrons leaving the trap, measured with the help of a multigrid analyzer, and the energy distribution $f_e(eV) \sim dI_e/dV$ of electrons in this flux, normalized to their maxima.

At low pressures in the discharge ($p < 10^{-4}$ Torr), the mean free path of electrons with energy $E_e > 10$ eV is on the order of or larger than the setup size; thus, these particles can perform bounce-oscillations between the magnetic mirrors. The measured spectral power densities of electric current and electric field oscillations revealed the generation of a noisy electromagnetic field with its maximum at a frequency of $f_{\text{bounce}} \approx 850$ kHz, which corresponds to the bounce-frequency of longitudinal oscillations involving discharge electrons with an energy of about 10 eV. Figure 8 exhibits the spectral power density of electric field oscillations in the plasma resonator, induced in the probing antenna at frequencies lying in the vicinity of the frequency of longitudinal oscillations performed by discharge electrons between the mirrors of the magnetic trap.

As the gas pressure in the discharge tube was increased, the amplitude of observed oscillations sharply decreased and the generation ceased to exist for $p \geqslant 10^{-3}$ Torr, when the electron mean free path became smaller than the length of the plasma resonator. Note that the position of generated 'lines' on the frequency scale was practically independent of the magnitude of B_0 and the trap mirror ratio $B_{\max}/B_0$, which, however, influenced the amplitudes of these oscillations. In addition, the dependence of the position of the 'line'

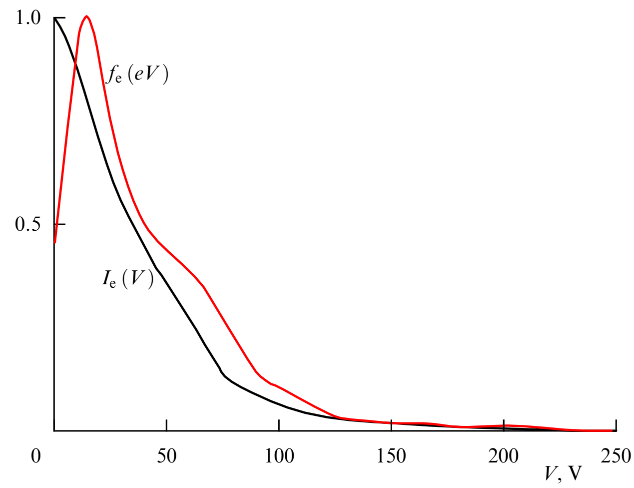

Figure 7. The dependence of discharge electron current to the collector of a multigrid analyzer on the retarding potential, $I_e(V)$, and the electron energy distribution function $f_e(eV)$, both normalized to respective maximum values.

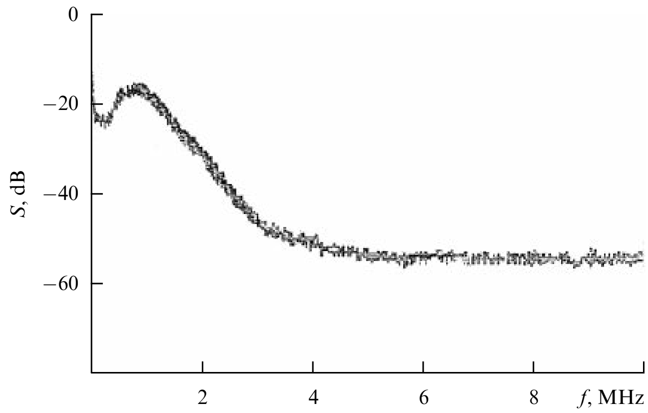

Figure 8. Spectral power density of noise oscillations of an electric field induced in the dipole antenna for $p < 10^{-4}$ Torr in the frequency range up to 10 MHz.

maximum on the pressure was discovered; specifically, at $p \approx 3 \times 10^{-4}$ Torr, the generation maximum (f_{bounce}) was displaced to a frequency of 0.6 MHz. This is seemingly related to some changes in the discharge regime and electron energy distribution in the plasma resonator.

A sharp increase in the level of power spectral density is also recorded in the frequency range of lower hybrid resonance (LHR) in cases where a signal from an auxiliary HF oscillator with the amplitude $V_{\mathrm{ext}} \sim 400$ V at a fundamental frequency of 3.4 MHz is applied to the quadrupole antenna located in the region of the mirror. When this oscillator was connected to an unmatched load, the spectrum of its signal comprised several harmonics. Figure 9 presents the noisy spectrum in the frequency range below 10 MHz, as averaged over a sufficiently long recording time and smoothed to remove bias signals at pressures $p \leqslant 10^{-4}$ Torr in the tube.

The dependence presented there shows a broadening of the spectrum maximum against the background of the first (3.4 MHz) and second (6.8 MHz) harmonics of the auxiliary HF oscillator signal, which corresponds, as discussed above, to the noise generation by bounce-electrons. A broad spectral line around 4 MHz is also apparent. Note that for the

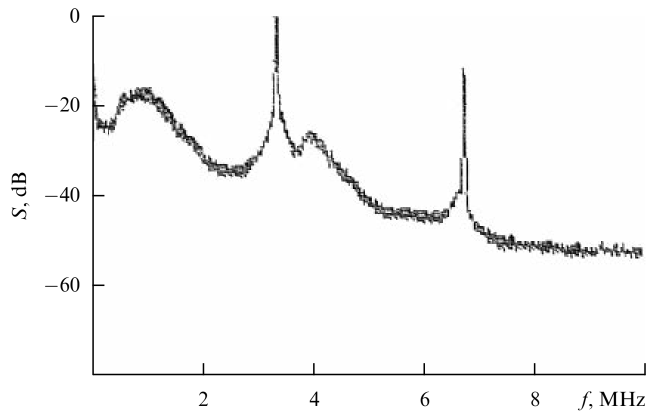

Figure 9. Spectral power density of electric field oscillations induced in the dipole antenna in the range of frequencies below 10 MHz in the discharge plasma for $p < 10^{-4}$ Torr in the presence of a signal from the auxiliary HF oscillator.

discharge plasma parameters given above, this frequency corresponds to the LHR frequency of a column of inhomogeneous plasma with concentration corresponding to concentration $\bar{N}(z)$ in the central part of the discharge channel.

Based on the analysis of the dispersion characteristics of a plasma waveguide in a nonuniform magnetic field [28], one may argue that at frequencies of ≈ 0.9 MHz the slowing-down of known axisymmetric waveguide modes is insufficient for their resonant excitation under the experimental conditions considered here. For this reason, we attribute the generation of oscillations observed by us to the bunching of discharge thermal electron beam and excitation by the modulated particle beam of quasipotential oscillations in a resonator-type plasma volume formed by the discharge. The resonator separates the radiation of bunched particles with velocities determined by the size of the plasma volume from the thermal noise at the eigenfrequency of beam oscillations. In the first turn, the maximum related to the most typical thermal velocity of electrons is distinguished. Such particles are most abundant in the discharge, and there always exist those which, being reflected in phase with field oscillations in the resonator, serve as centers of electron bunching. This fact allows one to estimate the electron temperature in the discharge by the observed noise emission peak. Indeed, the resonator size L_{r} and thermal velocity v_{Te} of electrons are related to the particular frequency f_{bounce} by the bounce-resonance relationship $L_{\mathrm{r}} = v_{\mathrm{Te}} \times (2 f_{\mathrm{bounce}})^{-1}$.

Under the conditions of our experiments, the estimated electron temperature at $f_{\mathrm{bounce}} \approx 800$ kHz is about 10 eV, which agrees well with the results of probe measurements.

When the auxiliary oscillator is switched on, a broad intense maximum in the vicinity of the frequency of ≈ 4 MHz, which corresponds to the frequency of lower hybrid resonance, is well discernible from the noise. The effective generation of this noise line is related first and foremost to the appearance of oscillating particles with a pump frequency of about 3.4 MHz in the discharge plasma. Moreover, beams of energetic electrons accelerated by the longitudinal electric field of the auxiliary high-frequency oscillator ($E_z \geqslant 50$ V cm^{-1}) are also produced. These highly energetic electrons are not abundant, but their amount grows markedly when the auxiliary oscillator is switched on, which entails an increase in the noise intensity in this frequency range. This is evidenced by electron spectra measured with a multigrid analyzer, which indicate that the electron retardation curve rises in the energy range around or higher than 100 eV when the auxiliary oscillator is operating.

The radiation intensity maximum occurs at the frequency of lower hybrid resonance because at this frequency the slowing-down of the waves, which is required to provide feedback ensuring the effective bunching of fast electrons and the resonance amplification of induced oscillations, is the strongest.

It should be noted that the relationships between characteristic frequencies of wave processes in laboratory experiments and under natural conditions [2] turned out to be such that the main similarity parameters $\omega/\omega_{\mathrm{pe}} \ll 1$, $\omega/\omega_{\mathrm{He}} \ll 1$, and $\omega/\nu_{\mathrm{e}} \gg 1$ in both cases satisfy the strong inequalities for typical dimensionless parameters, which define the qualitative character of phenomena observed in the plasma.

An important experimental fact manifested in natural conditions is the blurring of the region of LHR noise in the vicinity of the artificial wave duct [2]. In the laboratory experiment, the excitation of LHR noise was not observed in the discharge channel either in the absence of an additional stimulating source. These facts lend support to the conclusions of Ref. [29] on a possible excitation mechanism of LHR noise through nonducted whistlers experiencing reflection in the region of LHR. In all probability, the channeling of whistler radiation from the magnetosphere is made more efficient and its reflection in the region of LHR is reduced when the artificial duct of plasma density is formed.

5. Generation of ion-acoustic and ion-cyclotron oscillations

Ion-acoustic waves at altitudes of the Earth's outer ionosphere and magnetosphere can be excited as a result of the decay of a sufficiently powerful signal from a very low-frequency (VLF) transmitter into plasma and low-frequency ion-acoustic waves [30].

Damping of ion-acoustic waves influences the threshold of decay instability in an essential way. It is known that ion-acoustic waves are weakly damped if the temperature of electrons considerably exceeds that of ions, which is precisely what is observed in laboratory plasma where $T_e/T_i \sim 10$. Under ionospheric conditions, one finds $T_e/T_i \geqslant 1$. However, Ref. [30] argues that even in the latter case the decay of ion-acoustic waves can still be sufficiently weak, so that the development of decay instability for VLF waves would remain possible.

From Table 1, which compares the parameters of laboratory and ionospheric (at the altitude of the outer ionosphere) plasmas, one may infer that, judging by the main similarity parameters (see the last three rows of Table 1), the qualitative modeling of conditions in the Earth's outer ionosphere and the study of decay instability of waves in the whistler range are feasible in the plasma of a laboratory setup.

Table 1.

Parameter	Ionosphere (night)	Laboratory setup
	700 km	$p = 10^{-4}$ Torr
N_e, cm^{-3}	4×10^4	10^{10}
B_0, G	0.34	200
ν_e, s^{-1}	$\nu_{ei} \approx 55$	$\nu_{en} \approx 5.4 \times 10^5$
ω, s^{-1}	12.5×10^4	1.25×10^9
ω/ω_{He}	0.02	0.3
ω/ω_{pe}	0.012	0.2
ω/ν_e	2273	2314

To detect such low-frequency instabilities in this demonstration, we used a receiving antenna in the form of a symmetric electric dipole arranged close to the wall of a discharge tube. The receiving antenna was connected through a low-frequency filter and a coaxial cable to a DSO Classic-6000 digital storage oscilloscope, which enabled analysis of the spectral characteristics of the received signal. The discharge was formed through ionization self-channeling of plasma waves in the whistler frequency range, excited by a linear quadrupole antenna with the length $l_{a1} = 12$ cm. The HF power supplied to the discharge amounted to 10 W. The longitudinal magnetic field was generated by solenoids *1* (see Fig. 1); coils *2* of the solenoid were disconnected from the power supply, which led to forming a quasiuniform magnetic

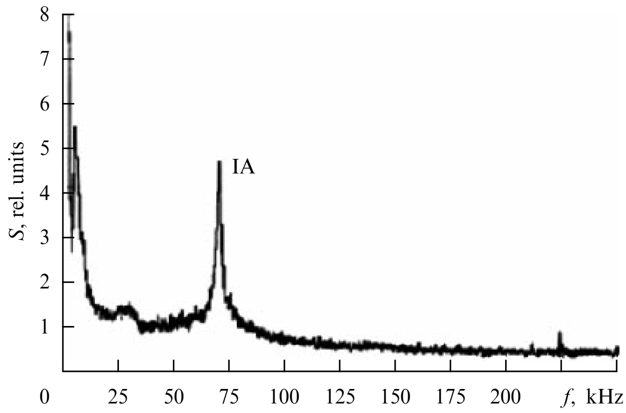

Figure 10. The spectrum of the low-frequency signal in a plasma for parameters $B_0 = 200$ G and $p \approx 10^{-4}$ Torr (IA stands for ion-acoustic waves).

field along the setup axis. The value of magnetic field induction, $B_0 = 200$ G, and pressure in the discharge chamber, $p \sim 10^{-4}$ Torr, were chosen in such a way as to ensure the most pronounced manifestation of observed effects. The nonuniformity of the magnetic field was below 10%.

The results of the demonstration are presented in Fig. 10 in the form of the dependence of spectral power density on the frequency of the received signal, $S(f)$. A maximum at the frequency $f_{IA} = 70$ kHz is well apparent in this dependence; it is related to the generation of ion sound.

To confirm this assumption, an additional experiment was carried out: a signal from a hydrophone put in a plastic bag filled with water and brought in contact with the discharge chamber was received by a sensitive AR-5000 low-frequency receiver. It turned out that the detectable signal agreed in its structure with that of the electric antenna, exhibiting a clearly expressed maximum at the frequency f_{IA}, while its frequency range was bounded by the hydrophone frequency characteristic. If the contact between water and the discharge chamber wall was disrupted, the signal from the hydrophone disappeared.

As the pressure was reduced, the resonance maximum shifted toward lower frequencies, $f \approx 60$ kHz. For $p > 6 \times 10^{-3}$ Torr, the generation of a maximum was not observed.

The efficiency of ion-acoustic wave generation decreased in a uniform magnetic field if a characteristic scale of the field nonuniformity approached the wavelength of the pump wave. This was manifested as smearing out of the intensity maximum at a distinguished frequency.

The spectrum of waves forming the discharge (the spectral density of HF field intensity is denoted as S_{HF}) was obtained and photographed with the help of the C4-27 high-frequency spectrum analyzer. The spectral lines of the pump field are shown in Figs 11a and 11b in the discharge plasma and without it, respectively.

Figure 11a displays the beatings of HF fields with several difference frequencies, among which $f_{IA} = 70$ kHz explicitly stands out. Broadening of the pump wave spectrum in the plasma as compared to the spectral line of the pump oscillator without a plasma load is also noticeable. For instance, the spectral width $\Delta_{-30}^{\text{plasma}} = 810$ kHz at the level of -30 dB, and $\Delta_{-30}^{\text{no plasma}} = 540$ kHz for the unloaded oscillator. Thus, the spectrum of the pump field became broader in the plasma by a factor of $\Delta_{-30}^{\text{plasma}}/\Delta_{-30}^{\text{no plasma}} = 1.5$.

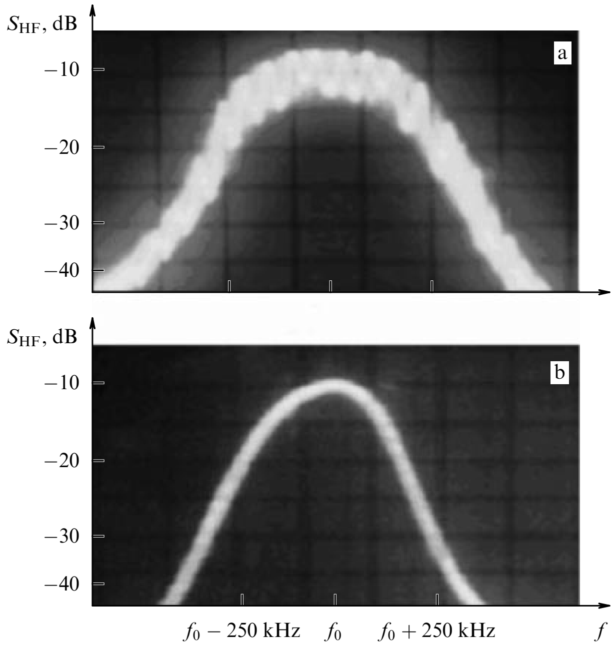

Figure 11. The spectral composition of HF fields (a) in the discharge plasma (the signal is attenuated by 20 dB), and (b) in the absence of plasma. One cell in the horizontal direction corresponds to 164 kHz.

The spectral width of the pump signal exceeds the frequencies of the modulation peaks. One can also see some asymmetry in the spectrum of radiation propagating in the plasma (it is broader on the 'red' side). A detailed analysis of the latter is given in Ref. [21]; here, we limit ourselves to explaining the effect of quasiresonant excitation of ion sound at a particular frequency.

Let us write out the conditions of decay interaction: $\omega_{1p} = \omega_{IA} + \omega_{2p}$, $\mathbf{k}_{1p} = \mathbf{k}_{IA} + \mathbf{k}_{2p}$. The dominant eigen wave of the plasma column, excited by the quadrupole source, is characterized by the following parameters: $\lambda_{1p} = 12$ cm and $f_0 = f_{1p} = 200$ MHz. The ion-acoustic eigen waves in this waveguide are characterized by the wavelength $\lambda_{IA} = 6$ cm according to calculated estimates made in Ref. [22]. Accordingly, one finds $\lambda_{2p} = 12$ cm from the decay conditions for the emerging high-frequency waves. In our experiments, the frequencies f_{1p} and f_{2p} lie within the spectral band of the pump signal. The effect of ion sound generation is, therefore, markedly enhanced through the beatings in the ponderomotive force of high-frequency pressure with relevant wave numbers k_{IA} and frequencies f_{IA} owing to the existence of spectral components in the pump signal that satisfy the synchronism conditions. The resonance peak of ion-acoustic wave excitation can be explained as follows. If the frequency of an ion-acoustic wave deviates from the values mentioned above, λ_{IA} varies, and so does λ_{2p} which is set by dispersion relations for the plasma channel. As a result, the decay conditions cease to be fulfilled for the eigen waves of the wave duct, while improper waves are excited less efficiently and damped more strongly.

The large number of peaks in Fig. 11a can be explained by cascade processes of scattering of the waves, which form the discharge from the excited plasma irregularities that are related to ion-acoustic oscillations. Thus, the low-frequency noise marked by the resonance peak (see Fig. 10) and the pump wave signal which underwent broadening (see Fig. 11) results from the decay processes in the pump field in the laboratory experiment. They can serve as a demonstration of spectral broadening effects for signals generated by very low-frequency (VLF) transmitters and of VLF noise generation in an artificial waveguide channel under natural conditions [2]. The effects of spectral broadening of the pump signal and increase in the level of LF noise, presented in Figs 5 and 6, are analogous to the data presented in Figs 10 and 11 and can also serve as demonstration of nonlinear processes in an artificial waveguide channel.

On reducing the pressure below $p \approx 10^{-4}$ Torr, the matching of the antenna with the surrounding medium under the conditions of discharge operation deteriorates and, as a consequence, plasma concentration N_e decreases. The outcome is that the same values of frequency correspond to larger values of the slowing-down factor in the dispersion characteristics. Therefore, the peak corresponding to 'resonance' excitation of ion sound shifts toward smaller frequencies to ensure the fulfillment of decay conditions. This is simultaneously accompanied by a reduction in amplitude and Q-factor for this maximum, yet together with the appearance of the possibility of observing the generation of a rich spectrum of low-frequency fields through the development of kinetic instabilities. These owe their existence to nonequilibrium distribution of charged particles over transverse velocities. The laboratory setup used here allows one to observe, for example, the generation of ion-cyclotron lines [32] driven by these instabilities. Both ions and resonance electrons whose thermal velocity is close to the phase velocity of the excited wave ($V_{Te} \sim \omega/k_z$) contribute to the excitation of ion-cyclotron oscillations.

In this demonstration the receiving dipole, which was attached to the surface of the discharge tube at its central part, was oriented along the z-axis and connected by a coaxial cable to the DSO Classic-6000 oscilloscope, which made possible determining the spectral characteristics of the received signal. The dependence of the spectral power density of the received signal on the frequency is presented in Fig. 12.

The spectrum plotted in Fig. 12 comprises three groups of lines with a fairly high Q-factor, which we attribute to ion-cyclotron resonances of the main plasma ions (singly, doubly, and triply charged). The gyrofrequencies of the dominant air ions (O_2, N_2) for the given experimental conditions are listed in Table 2. In addition, the spectrogram presented here allows one to discern a rather broad maximum related to the generation of ion-acoustic waves, and small resonance peaks

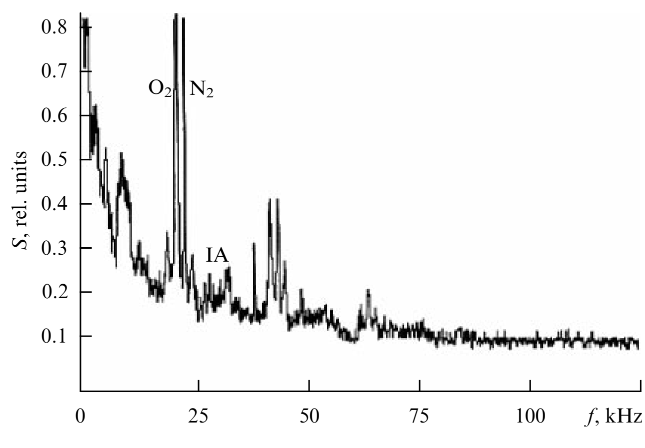

Figure 12. The spectrum of the low-frequency signal received by the dipole antenna in the range below 125 kHz at $p \approx 5 \times 10^{-5}$ Torr.

Table 2.

Ion	Frequency of observed generation $f_{\rm gen}$, Hz	Ion gyrofrequency $f_{\rm Hi}$, Hz
Molecular oxygen (O_2)	$20{,}000 \pm 1250$	20,023
Molecular nitrogen (N_2)	$22{,}500 \pm 1250$	22,884

at the noise level, which correspond to the lines of vacuum oil vapor, silicon, and metals. The Q-factor of observed lines increases with frequency. Accordingly, in the second and third groups of air ion-cyclotron lines, the line of nitrogen oxide is easily seen between those of oxygen and nitrogen. We remark that an increase in the pressure, $p > 10^{-4}$ Torr, or the switching off of the magnetic field in the mirrors of the magnetic trap destroyed the radiation emission at the characteristic resonance frequencies of the ions.

The intensity of the lines generated and their Q-factors depend on the HF power fed to the discharge, the magnitude of the magnetic field, the mirror ratio, and the pressure in the discharge tube. By varying these parameters one may control the parameters of the lines being excited. For instance, one can 'tune' to certain lines which will be distinguished among other lines by their intensity and Q-factors. The most convenient tuning parameters are the magnitude of the magnetic field and the mirror ratio. They can be varied in a fairly simple way within relatively wide intervals.

From a theoretical analysis of ion-cyclotron plasma instability [33] it follows that the instability growth rate γ is large ($\gamma \sim \omega_{\rm Hi}$) when the ion plasma frequency is high compared to the ion gyrofrequency, and the ion gyroradius $\rho_{\rm i}$ is not small compared to the transverse field scale ($k_{\perp}\rho_{\rm i} \geqslant 2.4$, $k_{\perp} \sim 2\pi/a$). Under the conditions of the experiments presented here, the cyclotron instability growth rate noticeably exceeds the collisional damping rate, whereas the resonance frequencies of oxygen and nitrogen ions turn out to be close to those observed in the experiment.

6. Conclusions

The experimental results presented here allow us to argue that the plasma-wave discharge in a linear mirror configuration of a magnetic field can be utilized for laboratory modeling and demonstrating magnetospheric nonequilibrium processes of electromagnetic radiation generation in a geomagnetic field tube with a duct of increased plasma density and for studying ionization self-focusing and the channeling of wave fields in the whistler frequency range. The laboratory setup can be employed as a kind of mass spectrometer for multiply charged ions.

The article provided descriptions of the following set of laboratory demonstrations:

— the resonance structure of an HF source field in a magnetoplasma;

— the self-focusing and channeling of wave fields in the whistler range for an HF discharge in the magnetic field;

— the models of a plasma resonator of the magnetospheric type;

— stimulated scattering of a pump wave from a lattice of plasma irregularities formed by the pump field;

— the excitation of lower hybrid and bounce resonances in the plasma resonator;

— the generation of ion-cyclotron and ion-acoustic instabilities in the plasma of the waveguide channel.

The descriptions given above allow one to reproduce the desired demonstration using a single laboratory facility by setting the following parameters: the required air pressure in the discharge chamber with the help of an air valve, the desired distribution of the magnetic field in the mirror trap through choosing the current in the solenoid coils, and the respective frequency ranges of analyzers for recording the effects to be observed.

The work was carried out with support from the RFBR (grant No. 07-02-00436a), the program Leading Scientific Schools NSh-1244.2008.2, the program Scientific and Scientific-Pedagogical Personnel of Innovative Russia (State contract No. P 1072), and the program Development of Scientific Potential of Higher Schools (2009–2010) (No. 2.1.1/1167).

References

1. Vas'kov V V et al. *Geomagn. Aeron.* **35** 98 (1995)
2. Rapoport V O et al. *Izv. Vyssh. Uchebn. Zaved. Radiofiz.* **50** 709 (2007) [*Radiophys. Quantum Electron.* **50** 645 (2007)]
3. Frolov V L et al. *Pis'ma Zh. Eksp. Teor. Fiz.* **88** 908 (2008) [*JETP Lett.* **88** 790 (2008)]
4. Milikh G M et al. *Geophys. Res. Lett.* **35** L17104 (2008)
5. Chugunov Yu V, Markov G A *J. Atmos. Solar-Terr. Phys.* **63** 1775 (2001)
6. Agafonov Yu N et al. *Pis'ma Zh. Eksp. Teor. Fiz.* **52** 1127 (1990) [*JETP Lett.* **52** 530 (1990)]
7. Alfvén H, Fälthammar C-G *Cosmical Electrodynamics* (Oxford: Clarendon Press, 1963) [Translated into Russian (Moscow: Mir, 1967)]
8. Podgornyi I M, Sagdeev R Z *Usp. Fiz. Nauk* **98** 409 (1969) [*Sov. Phys. Usp.* **12** 445 (1970)]
9. Starodubtsev M V, Nazarov V V, Kostrov A V *Phys. Rev. Lett.* **98** 195001 (2007)
10. Nazarov V V, Starodubtsev M V, Kostrov A V *Adv. Space Res.* **40** 390 (2007)
11. Gurevich A V *Usp. Fiz. Nauk* **177** 1145 (2007) [*Phys. Usp.* **50** 1091 (2007)]
12. Erukhimov L M et al. *Izv. Vyssh. Uchebn. Zaved. Radiofiz.* **30** 208 (1987) [*Radiophys. Quantum Electron.* **30** 156 (1987)]
13. Belikovich V V, Benediktov E A, Tolmacheva A V, Bakhmet'eva N V *Issledovanie Ionosfery s Pomoshch'yu Iskusstvennykh Periodicheskikh Neodnorodnostei* (Investigation of the Ionosphere by Artificial Periodic Irregularities) (Nizhny Novgorod: IPF RAN, 1999)
14. Frolov V L et al. *Izv. Vyssh. Uchebn. Zaved. Radiofiz.* **51** 915 (2008) [*Radiophys. Quantum Electron.* **51** 825 (2008)]
15. Markov G A, Mironov V A, Sergeev A M *Pis'ma Zh. Eksp. Teor. Fiz.* **29** 672 (1979) [*JETP Lett.* **29** 617 (1979)]
16. Bodrov S B, Markov G A *Fiz. Plazmy* **28** 1077 (2002) [*Plasma Phys. Rep.* **28** 992 (2002)]
17. Fisher R K, Gould R W *Phys. Rev. Lett.* **22** 1093 (1969)
18. Markov G A *Zh. Eksp. Teor. Fiz.* **113** 1289 (1998) [*JETP* **86** 703 (1998)]
19. Dobrokhotov V V, Markov G A *Izv. Vyssh. Uchebn. Zaved. Radiofiz.* **46** 392 (2003) [*Radiophys. Quantum Electron.* **46** 352 (2003)]
20. Belov A S, Markov G A *Fiz. Plazmy* **34** 252 (2008) [*Plasma Phys. Rep.* **34** 223 (2008)]
21. Markov G A, Khazanov I V *Fiz. Plazmy* **28** 307 (2002) [*Plasma Phys. Rep.* **28** 274 (2002)]
22. Belov A S, Markov G A *Fiz. Plazmy* **32** 826 (2006) [*Plasma Phys. Rep.* **32** 759 (2006)]
23. Mayhan J T et al. *J. Appl. Phys.* **42** 5362 (1971)
24. Gil'denburg V B, Kim A V *Zh. Eksp. Teor. Fiz.* **74** 141 (1978) [*Sov. Phys. JETP* **47** 72 (1978)]
25. Belikovich V V et al. *Izv. Vyssh. Uchebn. Zaved. Radiofiz.* **24** 504 (1981)

26. Bespalov P A, Trakhtengerts V Yu *Al'fvenovskie Mazery* (Alfvén Masers) (Gorky: IPF AN SSSR, 1986)
27. Belov A S, Markov G A, Popova L L, Chugunov Yu V *Geomagn. Aeron.* **49** 199 (2009) [*Geomagn. Aeron.* **49** 187 (2009)]
28. Kondratenko A N *Plazmennye Volnovody* (Plasma Waveguides) (Moscow: Atomizdat, 1976)
29. Jirícek F, Shklyar D R, Tríska P *Ann. Geophys.* **19** 147 (2001)
30. Kotik D S, Trakhtengerts V Yu *Geomagn. Aeron.* **13** 871 (1973) [*Geomagn. Aeron.* **13** 737 (1973)]
31. Grach S M *Izv. Vyssh. Uchebn. Zaved. Radiofiz.* **18** 1627 (1975) [*Radiophys. Quantum Electron.* **18** 1200 (1975)]
32. Dobrokhotov V V, Lyukshin N M, Markov G A, Chugunov Yu V *Fiz. Plazmy* **31** 701 (2005) [*Plasma Phys. Rep.* **31** 646 (2005)]
33. Mikhailovskii A B *Zh. Eksp. Teor. Fiz.* **44** 1552 (1963) [*Sov. Phys. JETP* **17** 1043 (1963)]